In Situ Microscope FTIRS Studies of CO Adsorption on an Individually Addressable Array of Nanostructured Pt Microelectrodes − An Approach of Combinatorial Analysis of Anomalous IR Properties

Hui Gong, Shi-Gang Sun,* You-Jiang Chen, and Sheng-Pei Chen

State Key Laboratory for Physical Chemistry of Solid Surfaces, Department of Chemistry, Institute of Physical Chemistry, Xiamen University, Xiamen 361005, China

Received: November 25, 2003; In Final Form: May 21, 2004

Combinatorial spectroelectrochemical analysis was carried out in the present paper by combining in situ microscope FTIR spectroscopy with an individually addressable array of Pt microelectrodes (ME_{ij}). A series of nanostructured films was created on the array through a treatment of fast potential cycling with varying duration (τ). STM studies illustrate that a nanostructured film is composed of Pt islands. The film thickness and island size increase consecutively on ME_{ij} of the array along with the increasing duration τ. Using CO adsorption as the probe reaction, anomalous IR properties of nanostructured films on the array were investigated systematically. It was revealed that anomalous IR properties depended strongly on the nanostructure of Pt thin films on the array. Following the increase of the film thickness and the size of Pt islands on the film, the IR features of CO linearly adsorbed (CO_L) on Pt microelectrodes of the array underwent the following various changes: (1) the spectral line shape of IR absorption of the CO_L species was changed from the negative-going monopolar band (normal IR absorption) to the bipolar band, and finally to the positive-going monopolar band; (2) the center of the CO_L band presented a volcano-type variation; that is, the positive-going CO_L band center ($\tilde{\nu}_{CO_L(\uparrow)}$) increased progressively from 2076 cm^{-1} to a maximum 2082 cm^{-1}, then decreased to 2070 cm^{-1}; (3) the stark tuning rate ($d\tilde{\nu}_{co}/dE$) of the CO_L band was decreased gradually; (4) the full width at half-maximum (fwhm) of the CO_L band reached the maximum at $\tau = 100$ min but, thereafter, decreased gradually; and (5) the enhancement of IR absorption of CO_L species was determined to yield the maximum 6.73 at $\tau = 100$ min. Besides the anomalous IR properties, the electrocatalytic activity of the array for CO oxidation was also studied by cyclic voltammetry. The present study has shed light on the intrinsic relationship between nanostructures of Pt film materials and anomalous IR properties as well as their electrocatalytic activity.

Introduction

The synthesis and characterization of nanomaterials have attracted extensive attention throughout the world. Their progress has been reported and reviewed in relevant fields in recent years.[1−8] Materials at the nanometer scale always exhibit unusual chemical, physical, and biological properties, which have a wide range of applications. Among them, the use of nanomaterials in electrocatalysis is one of the major interests.[8,9] For example, conductive substrate modified with nanometer particles of Pt-group metals are extensively used as electrocatalysts in direct methanol fuel cells (DMFC) for the reason of high activities and low costs.[10] The properties of nanometer scale materials are known to strongly depend on their size, shape, and composition. To gain a better understanding of nanometer scale materials serving as catalysts with respect to the origin of their high activity and selectivity in electrochemical reactions, it is indispensable to investigate the intrinsic relationship between physicochemical phenomena and nanostructures.

Electrochemical in situ infrared spectroscopy is a powerful technique that possesses high sensitivity on surface structures.[11,12] It has been successfully used to study the bonding and orientation of adsorbates,[13,14] the structure of the double layer at solid|liquid interfaces,[15,16] the mechanism of electrochemical oxidation of small organic molecules,[17,18] and the structure of polymer film formed on electrode.[19,20] Using this technique, Sun and co-workers[21−25] have systematically investigated the IR characteristics of adsorbed CO on nanostructured thin films of platinum group metals such as Pt, Pd, Rh, Ru, and their alloys. In their work, the nanostructured films were prepared by electrochemical methods, such as electrodeposition, to form metallic or bimetallic films on a conductive substrate such as glass carbon. Remarkably, they discovered that a CO molecule (CO_{ad}) adsorbed on the surface of two-dimensional nanometer-scale materials exhibited anomalous IR properties, that is, three abnormal IR characteristics in comparison to normal IR spectra for CO_{ad} on the surface of a bulk metal electrode: (1) the direction of CO_{ad} bands is completely inverted (abnormal IR absorption); (2) the IR adsorption of CO_{ad} is significantly enhanced; and (3) the full width at half-maximum (fwhm) of IR bands is considerably increased. This unusual IR phenomenon with nonlinearly optical characteristics was named the abnormal infrared effects (AIREs) by its discoverers.[25−27] Similar abnormal IR features were also reported for CO adsorbed on the electrodeposited thin film of Ir,[28] and Os[29] substrated on glass carbon and on platinized platinum surfaces.[30] To gain a better understanding of AIREs, it is crucial to systematically study the relationship between AIREs and

* Corresponding author. Telephone: +86 592 2180181. Fax: +86 592 2183047. E-mail: sgsun@xmu.edu.cn.

10.1021/jp0375822 CCC: $27.50
Published on Web 07/10/2004

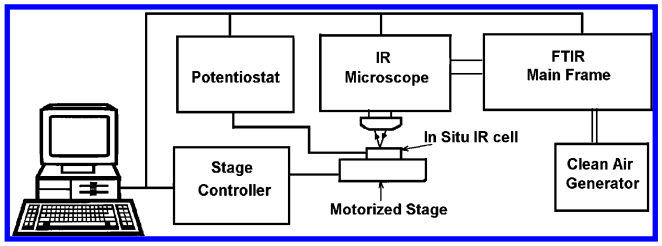

Figure 1. Block diagram of electrochemical in situ microscope FTIR spectroscopy (MFTIRS).

nanostructures. Although the observation of AIREs is now available using the technique of electrochemical in situ FTIRS, there are only few existing reports on the systematical study on the relationship between AIREs and nanostructures. The reason is that the previous studies were conducted on individual IR measurements, which has an unavoidable disadvantage in terms of data comparability.

Combinatorial chemistry is essentially based on the principle of parallelism.[31] It was initially applied in the discovery of new drugs with special properties,[32] but it has now made great progress in the field of solid-state studies, such as superconductive materials,[33] magnetoresistors,[34] photoluminescent materials,[35] catalysis,[36] and electrocatalysis.[10] A spatially addressable combinatorial technique is invariably used in these studies, which illustrates high advantage in terms of data comparability. This technique predicates a potential application in the exploitation of physicochemical properties with respect to nanostructures.

Recently, IR techniques were developed and a new technique called in situ microscope FTIR spectroscopy (MFTIRS) was established in our group.[37,38] The new IR technique has an advantage of spatial resolution that allows the IR detection of a microscale area and allows one to obtain a distribution of IR properties of the micro-area over the electrode surface. In a previous study in our group, the AIREs features of the CO probe molecule were observed on a nanostructured Pt microelectrode that was treated by a fast potential cycling (FPC).[38] On the basis of the combinatorial principle, a novel individually addressable array (3×3) of platinum microelectrodes was designed and fabricated in this paper, which was used to prepare different nanostructured surfaces through a FPC treatment with sequentially increased duration. Consequently, a combinatorial study of the variation of IR features correlated to nanostructures was conducted by combining the individually addressable array and in situ MFTIRS with CO as a probe molecule. Additionally, surface nanostructures of metal films were systematically studied by the ex situ STM technique.

Experimental Section

In Situ MFTIRS. Figure 1 illustrates the setup of in situ microscope FTIR reflection spectroscopy (in situ MFTIRS), which mainly consists of a Nexus 870 spectrometer (Nicolet), a microscope (IR-Plan Advantage, Spectra-Tech Inc.) equipped with a narrow-range mercury cadmium telluride detector (MCT-A, with the HgCdTe photodiode size of 250 μm $\times$ 250 μm) cooled with liquid nitrogen, and a motorized stage. The stage is controlled by a computer and can provide a facility of $X-Y$ scanning with a precision of 1 μm, which enables IR detection of any defined microscale area on a flat sample attached to the stage. Therefore, the requirement of multiple analyses on each microelectrode of an array is fulfilled. A 263 potentiostat/galvanostat (EG&G) was used to control the electrode potential in IR measurements. The entire system of in situ MFTIRS was

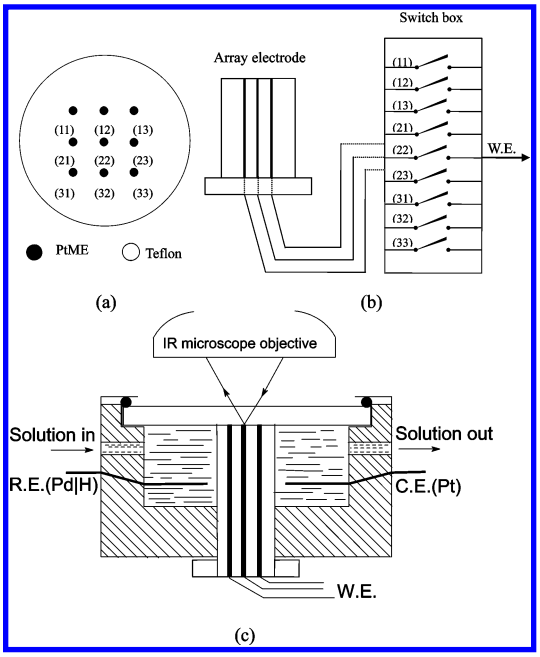

Figure 2. Illustrations of (a) a cross section of an individually addressable array of Pt microelectrodes; (b) the structure of the electronic switch component; and (c) the schematic structure of the electrochemical in situ IR cell.

run by the software written in our laboratory that communicates with the OMNIC software package (Nicolet), which permits not only control of the IR optical bench and IR microscope but also synchronization of the electrode polarization and spectral data collection. A video system attached to the IR microscope was used to visually inspect the surface of the microelectrode and to help adjust the microscope aperture that defines the incident IR beam in geometry and size. As the diameter of the Pt microelectrode is 200 μm (see below), the cross section of the incident IR beam in the current study was confined in a square size of 200 μm $\times$ 200 μm. The potential-difference method was employed in the IR measurements. The resulting spectrum was calculated as the relative change in reflectivity by the following formula,

$$\frac{\Delta R}{R} = \frac{R(E_S) - R(E_R)}{R(E_R)} \quad (1)$$

where $R(E_R)$ and $R(E_S)$ are single-beam spectra respectively collected at the reference potential E_R and the sample potential E_S. In this study, E_R was chosen at 1.00 V (vs Pd|H, CO is completely oxidized) and E_S was chosen at the potential of CO stable adsorption. According to eq 1, the negative-going feature of the CO_{ad} IR band would be expected to appear in the resulting spectra. To obtain a satisfactory single-to-noise ratio, 100 interferograms were collected and coadded into each single-beam spectrum. The spectral resolution was 8 cm^{-1}.

Individually Addressable Array of Platinum Microelectrodes and in Situ MFTIRS Cell. The structure of the array is shown in Figure 2. A Teflon template with nine holes arranged in a 3×3 array was made at first in a machine shop. Nine platinum wires of 200 μm in diameter were then filled into the holes and fixed with epoxy resin. To avoid electrochemical interference caused by overlapping of diffusion layers, the center-to-center distance between two neighboring Pt microelectrodes is set at 1.0 mm, which is 5 times as much as the size of a Pt microelectrode (PtME). For the sake of convenience, each individually addressable PtME in the array is assigned a

TABLE 1: ME_{ij} Subjected to the FPC Treatment for Different Duration Times (0 min ≤ τ ≤ 160 min)

ME_{ij}	ME_{11}	ME_{12}	ME_{13}	ME_{21}	ME_{22}	ME_{23}	ME_{31}	ME_{32}	ME_{33}
τ/min	0	20	40	60	80	100	120	140	160

matrix coordinate, for example, ME_{11}, ME_{12}, ME_{13}, etc., as shown in Figure 2a.

We varied progressively the size of the IR beam focused on the microelectrode surface from 400 μm × 400 μm to 40 μm × 40 μm through adjusting the variable rectangular aperture of IR microscope, and we found that when the size of the IR beam is larger than 200 μm × 200 μm, the IR signal of CO adsorbed on the Pt microelectrode reaches the maximum and keeps almost constant. The results indicate that the influence of Teflon surrounding the Pt microelectrode on the array during IR measurement can be negligible even when the IR beam size is much larger than the surface Pt microelectrode. However, to avoid possible interference of IR reflection from Teflon surrounding the Pt microelectrode, we limited the size of the IR beam focused on the microelectrode surface to 200 μm × 200 μm in all in situ MFTIRS measurements.

A homemade electronic switch box was specially designed to conveniently connect either all PtMEs together or any individual PtME or an arbitrary group of PtMEs with a potentiostat. The schematic design of the switch box is illustrated in Figure 2b.

The electrochemical in situ MFTIRS cell is schematically shown in Figure 2c. The cell body is made of Teflon. The counter and reference electrodes are platinum and palladium wires, respectively. The reference electrode of Pd was charged in saturation with hydrogen (Pd|H). All electrode potentials reported in this paper were quoted to the Pd|H electrode scale. To minimize the loss of IR incident energy by solvent (water) absorption, the microelectrode array was pushed toward the CaF_2 IR window until an optimal IR signal was obtained, so that a thin layer of electrolyte solution with a few micrometers in thickness between the array and the IR window was formed for in situ MFTIRS measurements.[39,40]

Other Conditions. The array of PtME (MEA) was polished with sand paper and alumina polishing powder of size 5, 1, 0.3, and down to 0.05 μm. After being washed in an ultrasonic bath, and thoroughly rinsed with Millipore water, the MEA was cleaned by potential cycling between 0.00 and 1.58 V in 0.1 mol L^{-1} H_2SO_4 at a scan rate of 0.10 V s^{-1}, until reproducible and well-defined Pt voltammograms were recorded. Each PtME was then subjected to a treatment of fast potential cycling (FPC) between 0.00 and 1.58 V at a scan rate of 30.00 V s^{-1} to generate a nanostructured thin film on the surfaces (see STM results bellow). The thickness of the nanostructured film could be easily adjusted by varying the duration time (τ) of FPC treatment. In the present study, the nine PtMEs of the array underwent FPC treatment with different τ values that were increased progressively from ME_{11} to ME_{33} and are listed in Table 1. As a consequence, an array composed of different nanostructured Pt films was prepared.

A scanning tunneling microscope of type P4-18-SPM (NT-MDT, Russia) was used to investigate in atmosphere the surface structures of MEA subjected to treatment of fast potential cycles.

All solutions were prepared with super pure H_2SO_4 and Millipore water purified in a Milli-Q Lab apparatus (Millipore Ltd., Japan). Adsorption of CO on MEA was carried out in CO saturation 0.1 mol L^{-1} H_2SO_4 solution. During CO adsorption, the electrode potential was cycled between 0.00 and 0.25 V at a scan rate of 0.10 V s^{-1} until the hydrogen adsorption current on PtMEs was completely suppressed due to saturation adsorption of CO. All experiments were performed at room temperature around 22 °C.

Results and Discussion

STM Studies. The surface structure of Pt microelectrodes on the array after having been subjected to the fast potential cycling treatment of different duration was studied ex situ with a scanning tunneling microscope. For comparison, STM patterns of the nine PtMEs on the array (see Figure 3a and b) were recorded with a same scan area of 4.0 × 4.0 μm^2. It can be clearly seen that the FPC treatment with different duration consequently changes the surface structure. Only scratches created during mechanical polishing and small platinum crystallites of about 40 nm could be observed on ME_{11}, the original PtME without FPC treatment. As the duration increases, the dimension of those Pt crystallites on PtME surfaces accordingly grows. The average size ($\bar{d}$) and average height ($\bar{h}$) of Pt islands in the film are measured to be 95 and 19.4 nm on ME_{12} at τ = 20 min, and 296 and 178 nm on ME_{23} at τ = 100 min. When τ continuously increases, $\bar{d}$ and $\bar{h}$ increase rapidly. We can see from Figure 3b that the thickness of nanostructured films formed on the surface of PtME has increased progressively from ME_{11} to ME_{33}.

The STM images may suggest that a process of fast electrodissolution and electrocrystallization must take place during the FPC treatment. It may be that an induction process has occurred on the PtME surface, that consequently leads to the formation of large Pt islands and, then, creates a nanostructured film on the surface.

With the help of statistical evaluation facilities in the STM software package, the average thickness ($\bar{l}$) of the nanostructured film for each PtME can be calculated by eq 2

$$\bar{l} = \frac{1}{n^2}\sum_{i=1}^{n}\sum_{j=1}^{n}|Z_{(i,j)}| \tag{2}$$

where $|Z_{(i,j)}|$ is the height of the pixel (i,j) in STM patterns. In the present study, n = 512, and a total of 512^2 = 262 144 points are involved in the calculation. Additionally, the root-mean-square of roughness average (R_q) for each PtME can be defined by eq 3.

$$R_q = \sqrt{\frac{1}{n^2}\sum_{i=1}^{n}\sum_{j=1}^{n}(Z_{(i,j)} - \bar{l})^2} \tag{3}$$

It is evident that R_q may be considered as an error in $\bar{l}$ measurements. Figure 4 displays the histogram of $\bar{l}$ and R_q of the PtMEs on the array. Figure 5 shows the variation of $\bar{d}$ and $\bar{h}$ of the PtMEs. The results demonstrate that the structural parameters including $\bar{l}$, R_q, $\bar{d}$, and $\bar{h}$ concurrently increase from ME_{11} to ME_{33} as the duration time becomes larger.

Electrochemical Characterization of Nanostructured Pt Films on the Array. Cyclic voltammetry was applied to investigate the electrochemical behavior of nanostructured PtMEs on the array. Figure 6a and b shows the comparison of voltammograms of PtMEs in 0.1 mol L^{-1} H_2SO_4 solution at a 0.10 V s^{-1} scan rate. Cyclic voltammograms in Figure 6a and b resemble CV characters of a Pt electrode, that is, (1) two pairs

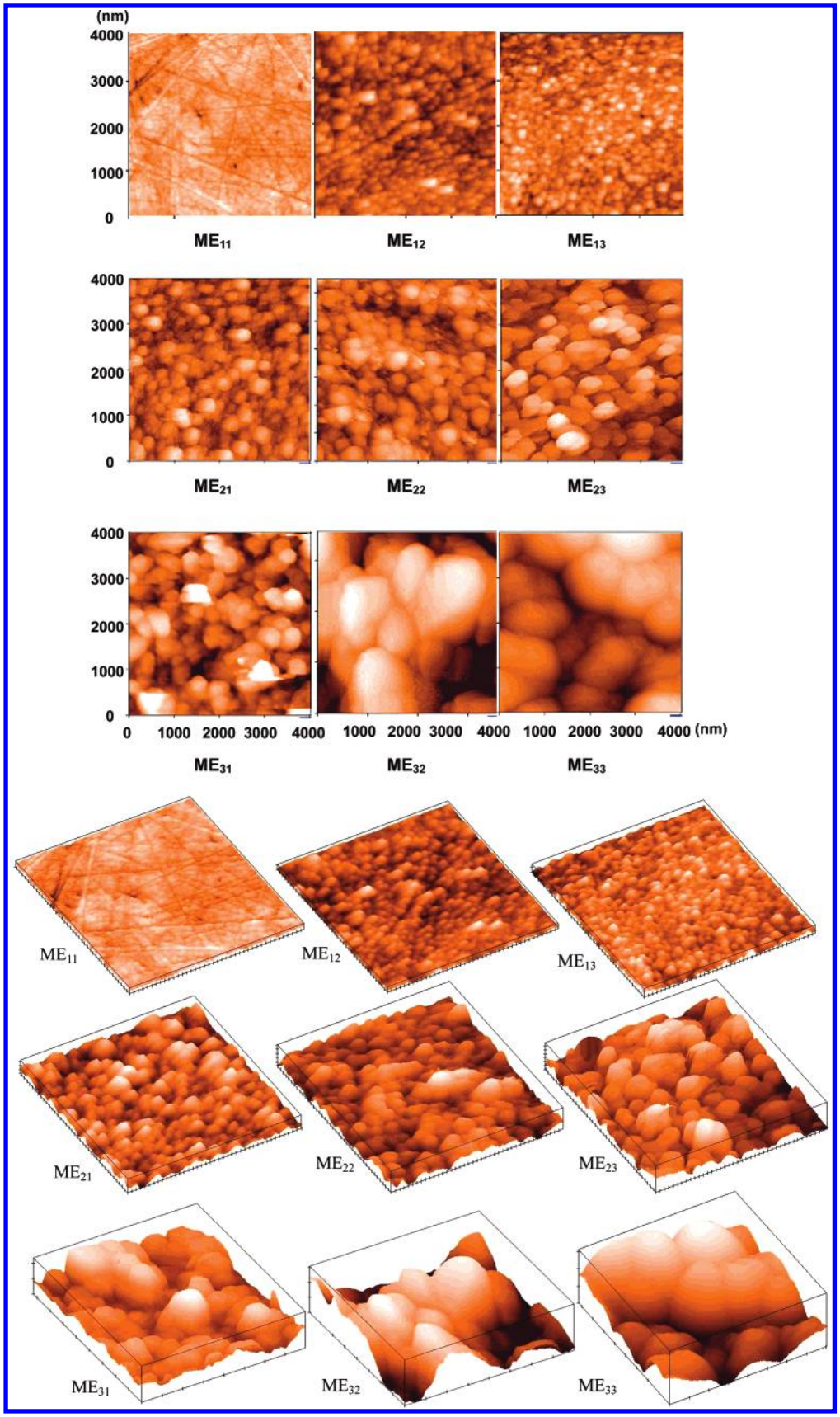

Figure 3. STM images of ME_{ij} on the array. (a) Two-dimensional presentations; (b) three-dimensional presentations, the former six images' scale: *X*, 100 nm, *Y*, 100 nm, *Z*, 100 nm; the latter three images' scale: *X*, 500 nm, *Y*, 500 nm, *Z*, 500 nm. Scan size: 4000 nm × 4000 nm; $I_t = 0.200$ nA, $V_b = 0.150$ V.

of current peaks located at around 0.09 and 0.25 V due to hydrogen adsorption/desorption, (2) the current peak of Pt oxidation above 0.79 V during the positive-going potential sweep, and (3) the reduction current peak of the Pt surface oxide near 0.95 V during the negative-going potential sweep. It was observed that the current in cyclic voltammograms gradually

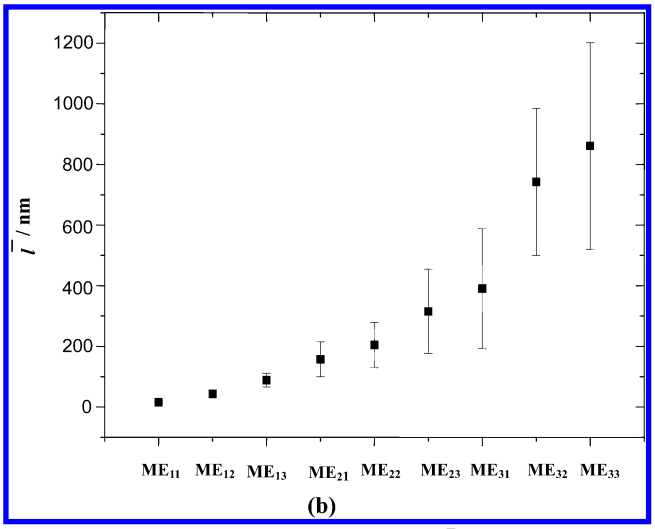

Figure 4. Variation of the average thickness ($\bar{l}$) and the root-mean-square of relative roughness average (R_q) of a Pt thin film of ME_{ij} on the array.

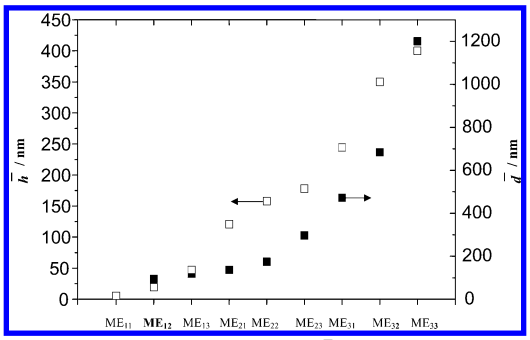

Figure 5. Variation of the average size ($\bar{d}$) and the average height ($\bar{h}$) of Pt islands in the Pt thin film of ME_{ij} on the array.

increases from ME_{11} to ME_{22} (Figure 6a), but reaches a near constant from ME_{23} to ME_{33} (Figure 6b). The pair of current peaks at around 0.09 V can be ascribed to hydrogen adsorption/desorption on the surface (111) or (110) sites of Pt, and that near 0.25 V can be ascribed to hydrogen adsorption/desorption on surface (100) sites of Pt.[41,42] It is interesting to note that current values of the latter pair increase faster than those of the former as duration times increase (Figure 6a). Prior to us, such an electrochemical phenomenon was already reported by other research groups. Arvia and co-workers observed that comparative increases in peak values of the two-pair current can occur when a technique called repetitive potential scan is used at a very high rate (about 10 000 V s^{-1}).[43−45] They ascribed such a phenomenon to a surface preferred crystallographic orientation. According to their results, CV curves shown in Figure 6a and b therefore manifest that FPC treatment is a kind of (100) faceting process, which results in a faceting of a particular surface structure for PtME. Obviously, the increasing voltammetric currents from ME_{11} to ME_{23} in Figure 6a must be related to increases of active surface areas of PtMEs because the geometric area of PtMEs remains unchanged throughout the FPC treatment. Therefore, it demonstrates that the surface of PtMEs became increasingly rougher as duration times increased within 100 min. The CV results could also confirm that an electrochemical process of fast electrocrystallization and electrodissolution has occurred at PtME surfaces, which led to the formation of nanostructured film and consequently an increase in the surface roughness of PtMEs that can be seen in STM images. However, the constancy of the current value from ME_{23} to ME_{33} in Figure 6b might imply that the magnitude of surface active sites for PtME reached a maximum when $\tau \geq 100$ min.

The electric charge corresponding to hydrogen adsorption (Q_H) on platinum is commonly used to evaluate the active surface area of Pt electrodes. It can be measured by means of integrating $j-E$ curves of the hydrogen adsorption region in the voltammogram of Pt electrodes. Thus, we define the relative roughness (R_r) as eq 4 by comparing the Q_H of treated PtMEs for varying duration times with that of the original PtME,

$$R_r = \frac{Q_H(\tau)}{Q_H(\tau = 0)} \tag{4}$$

The variation of R_r for PtME on the array is plotted in Figure 6c. For the purpose of summary, quantitative data of Q_H, R_r, $\bar{l}$, R_q, $\bar{d}$, and $\bar{h}$ obtained from STM studies are listed in Table 2. It can be seen that R_r gradually rises from ME_{11} to ME_{23}, and finally approaches a maximum beyond ME_{23}. The maximum value of R_r by FPC treatments is measured to be about 2.26, which is rather smaller than those reports written by other researchers, in which metal electrodes were usually subjected to a repetitive square-wave potential sweep treatment with a large potential window that extends into oxygen evolution.[46,47] In latter cases, the R_r can rise up to as high as 50−200. Our results here demonstrate that a FPC treatment prefers to generate a particular nanostructured film on the PtMEs having a relative low surface roughness.

It is worthwhile to note that R_q values obtained in STM images are different from R_r values obtained in CV curves, because R_q continuously increases, rather than approaching a maximum, as τ increases. It should be recognized that R_q measured from STM studies generally represents the physical parameter of surface unevenness; however, R_r measured from CV studies stands for the increment of surface active sites for hydrogen electrochemical adsorption. So R_r is a chemical parameter that significantly differs from R_q, although both of them can represent surface roughness. Our other results bellow will show that R_r should be used to evaluate the relative quantity of species adsorbed on a nanostructured PtME surface in comparison with that on the original PtME surface.

The cyclic voltammograms representing adsorption and oxidation of CO on ME_{ij} of the array are shown in Figure 7. The oxidation current of adsorbed CO (CO_{ad}) in the positive-going potential scan (PGPS) on bulk ME_{11}, that is, a PtME without FPC treatment, occurs in a sharp current peak at 0.862 V of amplitude 4.3 mA cm^{-1}. We cannot observe any oxidation current in the negative-going potential scan (NGPS), but a broad reductive current peak near 0.69 V due to the reduction of platinum oxides formed in PGPS. The oxidation of CO_{ad} on other ME_{ij} that has been treated by FPC with different duration illustrates that the onset potential (E_{onset}) of CO_{ad} oxidation is negatively shifted (as shown by the inset to the figure). The potential of the sharp oxidation current peak (E_p) is slightly postponed, and the amplitude of the current peak (j_p) is augmented.

The characteristic parameters E_{onset}, E_p, j_p, and the oxidation charge $Q_{oxi.}^{CO}$ that were measured by integration of the peaks of CO_{ad} oxidation in cyclic voltammograms are listed in Table 3. We can see that $Q_{oxi.}^{CO}$ is significantly increased from ME_{11} to ME_{23}, and thereafter levels off from ME_{23} to ME_{33}. It is noteworthy that this trend follows the pattern as Q_H that can be clearly seen in Table 2. This implies that the number of active surface sites for CO adsorption on a PtME surface increases as FPC treatment proceeds at the initial stage, but can reach a

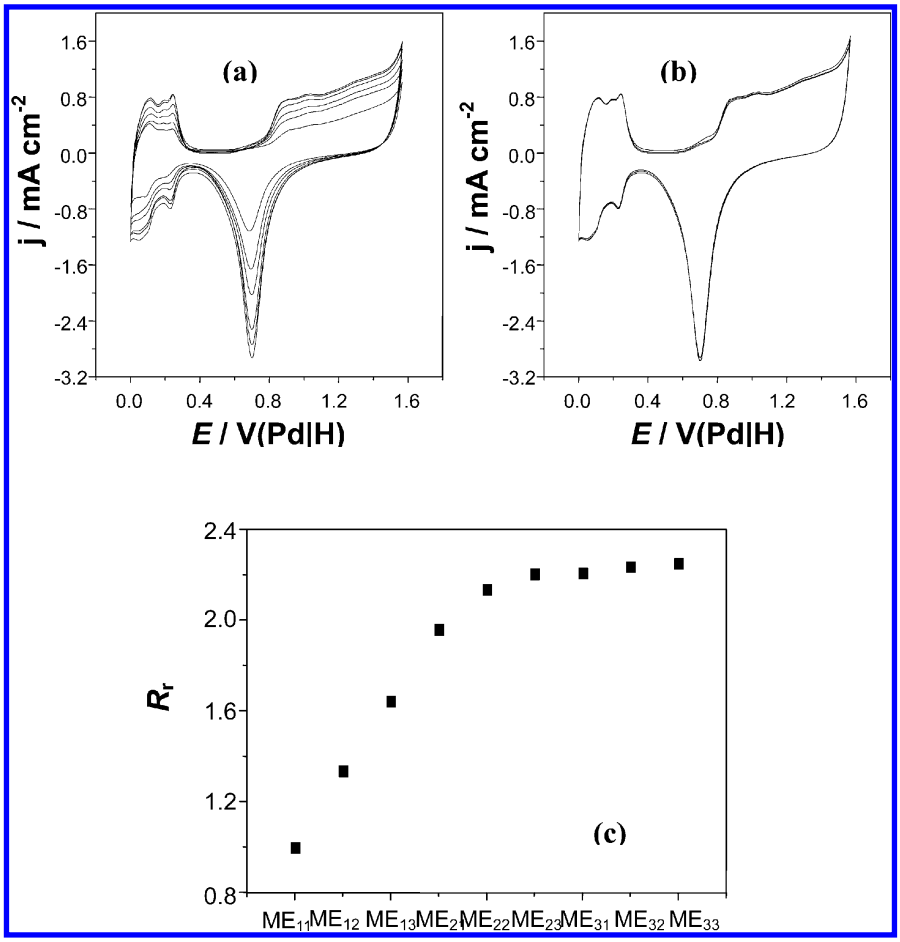

Figure 6. Cyclic voltammograms of ME_{ij} on the array in 0.1 M H_2SO_4 solution at a scan rate 0.10 V s^{-1}. (a) ME_{11} to ME_{22}, (b) ME_{22} to ME_{33} (τ = 100, 120, 140, 160 min), (c) distribution of surface relative roughness R_r over E_{ij}.

TABLE 2: List of CV and STM Parameters versus ME_{ij}

ME_{ij}	ME_{11}	ME_{12}	ME_{13}	ME_{21}	ME_{22}	ME_{23}	ME_{31}	ME_{32}	ME_{33}
$\bar{d}$/nm		95	118	136	174	296	472	683	1200
$\bar{h}$/nm	5.4	19.4	47.1	120.7	157.7	178	244.3	350	400
$\bar{l}$/nm	15.8	43	89	157	204	315	390	519	860
R_q/nm	4.8	13.3	22.6	57.7	74.4	139	198	242	341
Q_H/μC cm^{-1}	560.5	745.2	926.7	1098.7	1203.8	1235.6	1245.2	1257.9	1264.3
R_r	1.00	1.34	1.65	1.96	2.14	2.21	2.22	2.25	2.26

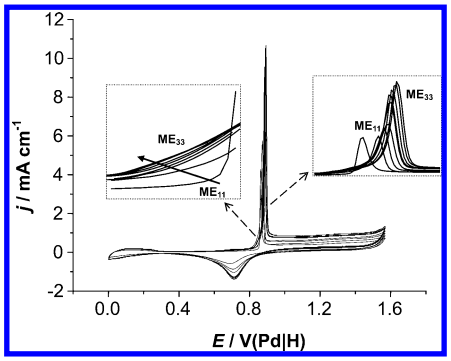

Figure 7. Cyclic voltammograms of CO adsorption and oxidation for ME_{ij} on the array, 0.1 M H_2SO_4 solution saturated with CO, scan rate 50 mV s^{-1}.

maximum when τ exceeds 100 min. These results described above indicate once again that although the increase in a FPC treatment can lead to the monotonic increase $\bar{l}$ of nanostructured films on PtME as shown in STM images, the number of the active surface sites for adsorption of CO or of hydrogen tends to reach a maximal limit when τ >100 min. The development of the reduction current peaks seen in cyclic voltammograms in Figure 7 can also confirm this point. As the geometric surface area of PtMEs on the array remains a constant value (3.14×10^{-4} cm^2) in FPC treatment, the relative surface roughness of PtMEs on the array also could be calculated by comparing the $Q_{oxi.}^{CO}$ measured on each ME_{ij} with that of ME_{11}, that is,

$$R_r' = \frac{Q_{oxi.}^{CO}(\tau)}{Q_{oxi.}^{CO}(\tau = 0)} \tag{5}$$

The variation of $R_{r'}$ with ME_{ij} listed in Table 3 is in good agreement with that of R_r illustrated in Table 2. The largest value of the $R_{r'}$ is calculated to be 2.66, which is slightly larger than that of R_r (2.26).

The Study of in Situ MFTIRS. CO adsorbed on the array of nanostructured Pt films in 0.1 M H_2SO_4 solution has been determined by in situ MFTIRS. According to the definition of eq 1, the IR spectral appearance must be dependent on the reference potential selected. Under the present conditions, wherein CO is adsorbed at E_S and completely oxidized at E_R (1.00 V), a negative-going band will be expected in the resulting spectra. In the spectrum of a bulk PtME, we have observed a

TABLE 3: List of CV Parameters versus ME_{ij} toward CO_{ad} Oxidation

ME_{ij}	ME_{11}	ME_{12}	ME_{13}	ME_{21}	ME_{22}	ME_{23}	ME_{31}	ME_{32}	ME_{33}
E_{onset}/V	0.854	0.839	0.834	0.833	0.830	0.828	0.827	0.827	0.827
E_p/V	0.862	0.876	0.880	0.883	0.885	0.887	0.887	0.889	0.891
j_p/mA cm^{-1}	4.3	4.4	5.3	5.8	8.2	9.0	9.6	10.5	10.7
Q_{oxi}^{CO}/μC cm^{-1}	980.9	1028.7	1493.6	1952.2	2519.1	2592.4	2598.7	2605.1	2611.5
R_r'	1.00	1.05	1.52	1.99	2.57	2.64	2.65	2.66	2.66

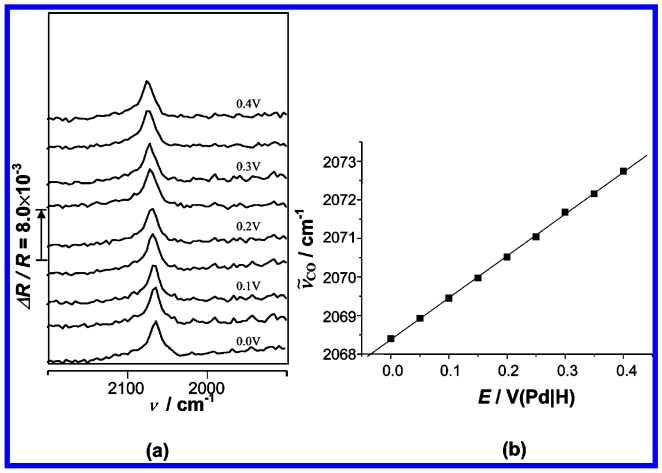

Figure 8. Potential dependence of in situ MFTIR spectra of CO_{ad} on PtME ($\tau \approx 160$ min). (a) Variation of in situ IR spectra of CO_{ad} with potential. (b) The center of the CO_L band as a function of potential. 0.1 M H_2SO_4 solution saturated with CO, $E_R = 1.00$ V, E_S is indicated in the figure.

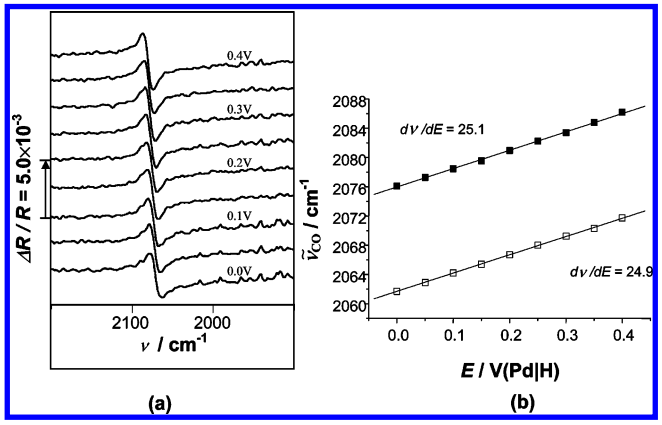

Figure 9. Potential dependence of in situ MFTIR spectra of CO_{ad} on PtME ($\tau \approx 50$ min). (a) Variation of in situ IR spectra of CO_{ad} with potential. (b) The center of the CO_L band as a function of potential. Solid and empty blocks represent the positive-going peak and the negative-going peak of the CO_L bipolar band. 0.1 M H_2SO_4 solution saturated with CO, $E_R = 1.00$ V, E_S is indicated in the figure.

negative-going band as expected near 2071 cm^{-1}, which is assigned to the IR adsorption of linearly bonded CO (CO_L) to the surface of a PtME. This IR feature is in good agreement with that observed on a conventional disk electrode of bulk Pt.[48]

Except for normal spectral features of CO on bulk PtME, we have observed two other types of CO spectra on nanostructured Pt films. To elucidate them, two kinds of CO spectra for PtME treated for 160 and 50 min are taken as examples in this paper, which are shown in Figures 8 and 9, respectively. Figure 8a exhibits the variation of CO spectra for PtME ($\tau = 160$ min) with E_S determined in 0.1 M H_2SO_4 saturated by CO. The IR band centered at around 2070 cm^{-1} is ascribed to CO_L species absorption. In comparison to bulk platinum, the direction of the CO_L band is obviously inverted and the intensity of this CO_L band is increased, which can be attributed to the AIREs. Such features will be described in detail in the following paragraphs of this paper. Beyond these, it can also be seen that the center of the CO_L band shifts to higher wavenumber as the potential increases. Such a potential-dependent shift was plotted in Figure 8b. The stark tuning rate ($d\tilde{\nu}_{CO_L}/dE$) for PtME ($\tau = 160$ min) can be obtained from the straight line to be 10.8 cm^{-1} V^{-1}, which is smaller than the value (30 cm^{-1} V^{-1}) measured for CO_L adsorbed on bulk Pt electrode, that is, ME_{11}. Figure 9a shows the variation of CO spectra for a PtME ($\tau = 50$ min) under the same conditions with that shown in Figure 8. To our surprise, CO_L IR absorption comes out as a bipolar band in this case, which is obviously different from both normal absorption and AIREs for which only the monopolar shape of the CO_L band appears in the latter two cases. It can also be seen that both centers of the positive- and negative-going peak of CO_L bipolar are blue-shifted with an increase of the potential. $d\tilde{\nu}_{CO_L}/dE$ values for the positive- and negative-going peaks are both around 25 cm^{-1} V^{-1}, which can be obtained from Figure 9b. It is known that the bipolar IR feature reflects the Fano-like spectral line shape.[49−51] The present results demonstrated that the Fano-like spectral line shape of CO_L is the representation of the particular IR property of defined nanostructure of the Pt thin film.

For the purpose of further understanding IR features for CO adsorbed on nanostructured Pt films, we carried out combinatorial studies of the serially nanostructured ME_{ij} array prepared in this paper by in situ MFTIRS. To easily compare their IR features, the resulted spectra obtained at a potential of 0.20 V are shown in Figure 10. Thus, the spectra in Figure 10 recorded on ME_{ij} on the array can illustrate the evolution of IR features for CO adsorbed on different nanostructures. The results can be itemized as follows:

(1) The first result is the evolution of the line shape of the CO_L band. Following the increase of τ, that is, from ME_{11} to ME_{33}, the CO_L band is illustrated as the negative-going monopolar band on ME_{11}, and then becomes a bipolar band on ME_{12}, ME_{13}, ME_{21}, and ME_{22} and finally changes into a positive-going band on ME_{23} to ME_{33}. Figure 10 clearly demonstrated a dramatic change in IR features, that is, from the negative-going monopolar band (normal IR absorption) to the bipolar band, and then to the positive-going monopolar band (abnormal IR absorption) of CO_L depending on the increase of the thickness of the nanostructured film and the size of the Pt islands in the film on the PtME surface. The transition range of the nanostructure of the Pt thin film yields both normal and abnormal absorption showing a bipolar feature of the CO_L band, that is, the Fano-like spectral line shape.

(2) The second result is the shift of the CO_L band center ($\tilde{\nu}_{CO_L}$). Figure 11 shows variations of wavenumbers at the positive-going band $\tilde{\nu}_{CO_L(\uparrow)}$ and the negative-going band $\tilde{\nu}_{CO_L(\downarrow)}$ with different PtMEs on the array. The hollow and solid circles in the graph represent the negative-going band $\tilde{\nu}_{CO_L(\downarrow)}$ and the positive-going band $\tilde{\nu}_{CO_L(\uparrow)}$, respectively. For the bipolar band in ME_{12}, ME_{13}, ME_{21}, and ME_{22}, both $\tilde{\nu}_{CO_L(\uparrow)}$ and $\tilde{\nu}_{CO_L(\downarrow)}$ of the two peaks are shown. In comparison with $\tilde{\nu}_{CO_L(\downarrow)}$ on the ME_{11}, that is, the bulk PtME, the negative-going band is all red-shifted, while the positive-going band is all blue-shifted except for that of the ME_{33}. We observe that the variation of $\tilde{\nu}_{CO_L(\uparrow)}$ with ME_{ij}

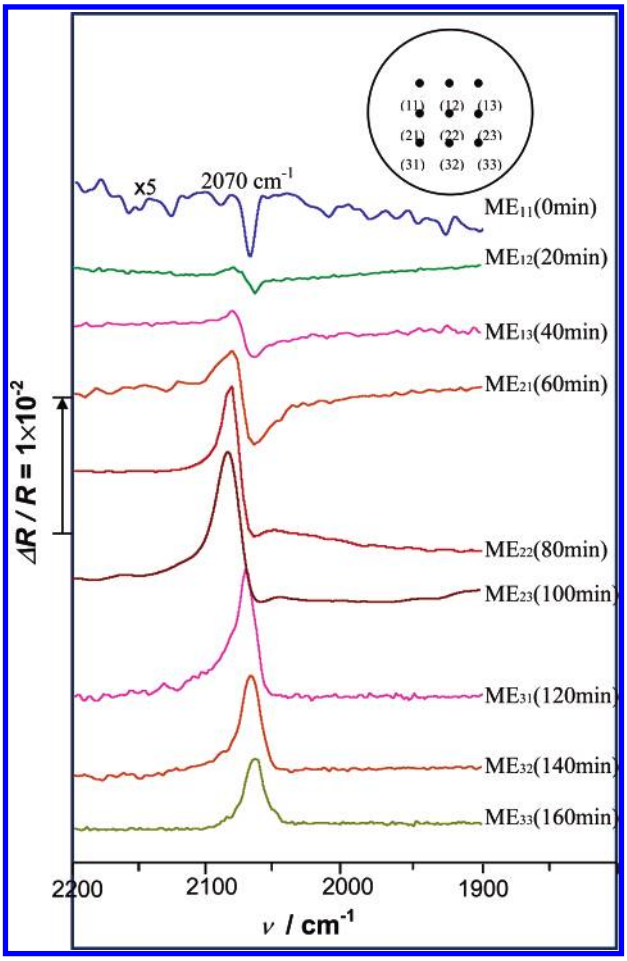

Figure 10. Comparison of in situ MFTIR spectra of CO_{ad} for ME_{ij} on the array. $E_R = 1.00$ V, $E_S = 0.20$ V, 0.1 M H_2SO_4 solution saturated with CO.

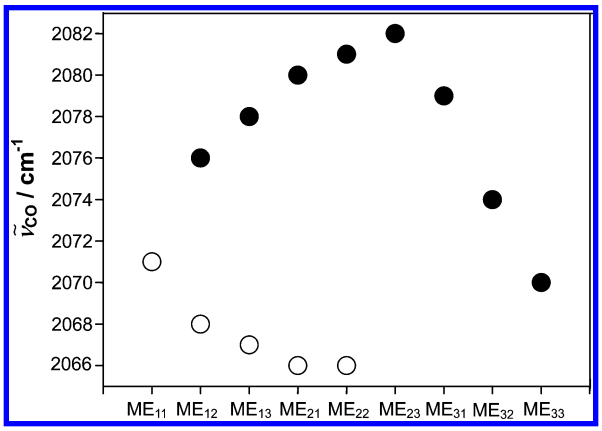

Figure 11. Variation of the CO_L band center versus ME_{ij}. Empty circles represent the negative-going CO_L band, and solid circles represent the positive-going CO_L band.

exhibits a volcano-type curve; that is, $\tilde{\nu}_{CO_L(t)}$ is increased initially from ME_{11} to ME_{23}, and then decreased from ME_{23} to ME_{33}, showing the maximum value of 2082 cm^{-1} measured on the ME_{23} which corresponds to $\tau = 100$ min ($\bar{d} = 296$ nm and $\bar{h} = 178$ nm).

(3) The third result is the change of the stark tuning rate ($d\tilde{\nu}_{co}/dE$). Figure 12 shows the variations of $d\tilde{\nu}_{co}/dE$ of the CO_L band on ME_{ij} of the array. The hollow and solid blocks in the graph represent $d\tilde{\nu}_{co}/dE$ of the negative-going peak and positive-going peak, respectively. $d\tilde{\nu}_{co}/dE$ is gradually decreased from ME_{11}

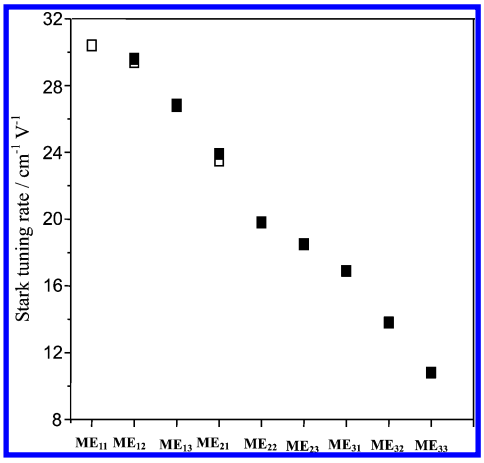

Figure 12. Variation of the stark tuning rate of the CO_L IR band for ME_{ij} of the array. Solid and empty blocks represent the positive-going band and the negative-going band, respectively.

to ME_{33}. It was noteworthy that $d\tilde{\nu}_{co}/dE$ of the negative-going part and positive-going part in one bipolar band are nearly equal.

(4) The fourth result is the variation of the bandwidth. The full width at half-maximum (fwhm) of the CO_L band increases up to 34.2 cm^{-1} on ME_{23}. This value is nearly 3 times that obtained on ME_{11} where the fwhm is measured to be 13.2 cm^{-1}. This result may imply that there are many more different surface sites formed on nanostructured ME_{ij}, which lead to the inhomogeneous broadening of the CO band.[52] The value of fwhm gradually decreases from ME_{23} to ME_{33}. The fwhm value for ME_{33} is 17.9 cm^{-1}, which is merely 4.7 cm^{-1} larger than that for the bulk PtME.

(5) The fifth result is the enhancement of IR absorption. In situ FTIR spectra in Figure 10 show that the intensity of the CO_L band increases in ME_{ij} that were subjected to FPC treatment. To study quantitatively the enhancement of IR absorption, an enhancement factor (Δ_{IR}) is designated to correlate the degree of enhancement to the nanostructure of each ME_{ij} as described in eq 6,

$$\Delta_{IR} = \frac{1}{R_r} \cdot \frac{A_{CO}(ME_{ij})}{A_{CO}(ME_{11})} \qquad (6)$$

where A_{CO} is the integrated intensity of the CO_L band. As it is not convenient to integrate the intensity of the CO_L bipolar band, only the enhanced positive-going CO_L band has been taken into account. Δ_{IR} was measured to be 6.73, 6.37, 5.46, and 4.23 from ME_{23} to ME_{33}, respectively. The maximum value observed on ME_{23} indicates that it has the largest enhancement of IR absorption among those nanostructured films on the array prepared in this paper.

The parameters of these IR characteristics of the CO_L band are summarized in Table 4. It is interesting to note that the ME_{23} possess the maximum enhancement factor Δ_{IR} coinciding with the highest band shift $\tilde{\nu}_{co}$ (Figure 11). The appearance of the CO band on ME_{ij} with $\tau \geq 100$ min clearly confirmed that the nanostructured film grown on PtME yields abnormal infrared effects (AIREs) that have been discovered by Sun and co-workers.[21−26] The present AIREs resembles abnormal IR features that occurred when CO and other molecules (SCN^-, CN^-, POPD, etc.) chemisorbed on nanostructures produced by depositing a nanometer-scale thin film of platinum group metals or alloys on glass carbon or other conductive substrates. Sun and co-workers have reported that in the case of CO adsorbed on nanometer-scale thin Pt film with GC as substrate produced

TABLE 4: List of IR Features of CO_L Bands versus ME_{ij}

ME_{ij}	ME_{11}	ME_{12}	ME_{13}	ME_{21}	ME_{22}	ME_{23}	ME_{31}	ME_{32}	ME_{33}
$d\tilde{\nu}_{CO(\uparrow)}/dE/cm^{-1}\ V^{-1}$		29.6	26.9	23.9	19.8	18.5	16.9	13.8	10.8
$d\tilde{\nu}_{CO(\downarrow)}/dE/cm^{-1}\ V^{-1}$	30.4	29.4	26.8	23.5	19.8				
$\tilde{\nu}_{CO_L(\uparrow)}/cm^{-1}$		2076	2078	2080	2081	2082	2078	2074	2070
$\tilde{\nu}_{CO_L(\downarrow)}/cm^{-1}$	2071	2068	2067	2066	2066				
$fwhm/cm^{-1}$	13.2					34.2	22.6	19.8	17.9

by the depositing technique of electrochemical cyclic voltammetry, the maximum value of Δ_{IR} was calculated to be about 20-fold.[26] They also observed that the positive-going direction of the CO band and the increase of CO bandwidth are maintained in all of the Pt thin film, which are independent of thickness. Our observation of both bipolar and positive-going monopolar bands of CO_{ad} in this paper actually expends our understanding of the IR special properties for nanostructured material and thus will be of helpful in revealing the origin of the AIREs.

It is worthwhile mentioning that the change in IR band direction from negative-going to bipolar, then to positive-going was observed first by Bjerke et al.[30] on platinized platinum electrodes prepared under constant voltage or constant current with successively increasing electroplating time. The results in this paper and those in the mentioned literature revealed that the anomalous IR properties depend strongly on the nanostructure of the film material and depend hardly on the material of the substrate.[53] It is evident that the combinatorial studies in the present paper exhibit a significant advantage of data comparability and research efficiency, which makes it possible to gain systematic and detailed information on nanostructures and their anomalous IR features.

Conclusions

An individually addressable PtMEs array was designed and fabricated in this work. A treatment of fast potential cycles was applied to each PtME on the array for different duration to yield a set of progressively varied surface nanostructures. The serially nanostructured array was then investigated using STM, cyclic voltammetry, and in situ microscope FTIR spectroscopy (MFT-IRS). It was observed that a nanostructured film could be produced at the microelectrode surface by such treatment. By comparing the patterns of STM image, we observed that both the thickness $\bar{l}$ of Pt thin film and the size $\bar{d}$ of Pt islands in the film increase with the increase of duration time. In the experiment of cyclic voltammetry, it was found that the charge of adsorption/desorption of H-adatoms increases in the initial stage of the treatment and reaches a maximum value of 2.26 in successive treatment. This result demonstrated that the treatment of a fast potential cycling led to a particular nanostructured film on the PtME with a relative low electrochemical roughness. By comparing onset potentials of CO_{ad} oxidation in CVs recorded on the individually addressable PtME array, we could draw the conclusion that the reactivity of the PtME surface for CO oxidation can be augmented upon such treatment.

The combinatorial study of IR properties of nanostructured PtMEs on the array for CO adsorption was carried out by electrochemical in situ microscope FTIR spectroscopy. The combination of the array and in situ MFTIRS provided a combinatorial spectroelectrochemical analysis, which exhibits a significant advantage of data comparability and research efficiency. A set of in situ MFTIR spectra was recorded on the array and under the same conditions. The results illustrated that the IR features of CO_L band progressively varied with the surface nanostructures of ME_{ij} on the array. The interesting changes include: (1) the direction and shape of the CO_L band is turned from the downward (normal absorption) and monopolar to bipolar (Fano-like spectral line shape), and finally to upward and monopolar (abnormal absorption); (2) the wavenumber of the positive-going band of CO_L underwent mainly two procedures, blue-shifted first, and then red-shifted, while the negative-going band of CO_L was always red-shifted; (3) the fwhm of the CO_L band is broadened in the sequence of serially nanostructured ME_{ij} on the array; (4) the change of stark tuning rates ($d\tilde{\nu}_{co}/dE$) is progressively decreased; and (5) the intensity of the CO_L band is enhanced at first, then decreased. These results illustrated clearly that following the increase of $\bar{l}$ and $\bar{d}$, the IR property of the nanostructured Pt film was reflected by a transition from absorption IR features to Fano-like spectral line shapes, and further to abnormal IR features.

We have developed a combinatorial spectroelectrochemical analysis method and shed valuable insights into revealing the intrinsic relationship law between the nanostructure of the Pt film material and the corresponding anomalous IR properties as well as electrocatalytic properties.

Acknowledgment. This work was supported by grants from the National Natural Science foundation of China (90206039, 20021002) and by the "973" program (2002CB211804). We are grateful to Dr. Yuanl Chow, professor emeritus from Simon Fraser University, for valuable discussions.

References and Notes

(1) Froba, M.; Reller, A. *Prog. Solid State Chem.* **1999**, *27*, 1.
(2) Lue, J.-T. *J. Phys. Chem. Solids* **2001**, *62*, 1599.
(3) Haruta, M.; Date, M. *Appl. Catal., A* **2001**, *222*, 427.
(4) Johnson, B. F. G. *Coord. Chem. Rev.* **1999**, *190−192*, 1269.
(5) Brust, M.; Kiely, C. *Colloids Surf., A* **2002**, *202*, 175.
(6) Grieve, K.; Mulvaney, P.; Grieser, F. *Curr. Opin. Colloid Interface Sci.* **2000**, *5*, 168.
(7) Hodak, J. H.; Henglein, A.; Hartland, G. V. *J. Phys. Chem. B* **2000**, *104*, 9945.
(8) Bo, A.; Sanicharane, S.; Sompalli, B.; Fan, Q.; Gurau, B.; Liu, R.; Smotkin, E. S. *J. Phys. Chem. B* **2000**, *104*, 7377.
(9) Park, S.; Yang, P.; Corredor, P.; Weaver, M. J. *J. Am. Chem. Soc.* **2002**, *124*, 2428.
(10) Reddington, E.; Sapienza, A.; Gurau, B.; Viswanathan, R.; Sarangapani, S.; Smotkin, E. S.; Mallouk, T. E. *Science* **1998**, *280*, 1735.
(11) Beden, B.; Lamy, C.; Bewick, A. *J. Electroanal. Chem.* **1981**, *121*, 343.
(12) Beden, B.; Lamy, C. Infrared Reflection Spectroscopy. In *Spectroelectrochemistry-Theory and Practice*; Plenum Press: New York and London, 1988; Chapter 5, p 189.
(13) (a) Chen, A.-C.; Yang, D.-F.; Lipkowski, J. *J. Electroanal. Chem.* **1999**, *475*, 130. (b) Li, H.-Q.; Roscoe, S. G.; Lipkowski, J. *J. Electroanal. Chem.* **1999**, *478*, 67. (c) Hoon-Khosla, M.; Fawcett, W. R.; Chen, A.-C.; Lipkowski, J. *Electrochim. Acta* **1999**, *45*, 611. (d) Chen, A.-C.; Sun, S.-G.; Yang, D.-F.; Pettinger, B.; Lipkowski, J. *Can. J. Chem.* **1996**, *74*, 2321.
(14) Li, W.-H.; Haiss, W.; Floate, S.; Nichols, R. J. *Langmuir* **1999**, *15*, 4875.
(15) (a) Marinkovic, N. S.; Hecht, M.; Loring, J. S.; Fewcett, W. R. *Electrochim. Acta* **1996**, *41*, 641. (b) Fawcett, W. R.; Kloss, A. A.; Calvente, J. J.; Marinkovic, N. *Electrochim. Acta* **1998**, *44*, 881.
(16) Ataka, K.; Osawa, M. *Langmuir* **1998**, *14*, 951.
(17) (a) Li, N.-H.; Sun, S.-G. *J. Electroanal. Chem.* **1997**, *436*, 65. (b) Li, N.-H.; Sun, S.-G. *J. Electroanal. Chem.* **1998**, *448*, 5. (c) Yang, H.; Lu, T.-H.; Xue, K.-H.; Sun, S.-G.; Lu, G.-Q.; Chen, S.-P. *J. Mol. Catal.* **1999**, *144*, 315. (d) Sun, S.-G.; Chen, S.-P.; Li, N.-H.; Lu, G.-Q.; Chen, B.-Z.; Xu, F.-C. *Colloids Surf.* **1998**, *134*, 207.

(18) Druliolle, H.; Koleoh, K. B.; Hahn, F.; Lamy, C.; Beden, B. *J. Electroanal. Chem.* **1997**, *426*, 103.
(19) Ping, Z.; Nauer, G. E.; Neugebuer, H.; Theiner, J.; Neckel, A. *J. Chem. Soc.* **1997**, *93*, 121.
(20) Nanbu, N.; Kitamura, F.; Ohsaka, T.; Tokuda, K. *J. Electroanal. Chem.* **1999**, *470*, 136.
(21) Lu, G.-Q.; Sun, S.-G.; Chen, S.-P.; Tian, Z.-W.; Yang, H.; Xue, K.-H. *Abstracts of the 189th ECS Meeting*; Los Angeles, May, 1996; p 1115.
(22) Lu, G.-Q.; Sun, S.-G.; Chen, S.-P.; Cai, L.-R. *J. Electroanal. Chem.* **1997**, *421*, 19.
(23) Lu, G.-Q.; Cai, L.-R.; Sun, S.-G.; He, J.-X. *Chin. Sci. Bull.* **1999**, *44*, 1470.
(24) Zheng, M.-S.; Sun, S.-G. *J. Electroanal. Chem.* **2001**, *500*, 223.
(25) Lin, W.-G.; Sun, S.-G.; Zhou, Z.-Y.; Chen, S.-P.; Wang, H.-C. *J. Phys. Chem. B* **2002**, *106*, 11778.
(26) Lu, G.-Q.; Sun, S.-G.; Cai, L.-R.; Chen, S.-P.; Tian, Z.-W.; Shiu, K.-K. *Langmuir* **2000**, *16*, 778.
(27) Chen, W.; Sun, S.-G.; Zhou, Z.-Y.; Chen, S.-P. *J. Phys. Chem. B* **2003**, *107*, 9808.
(28) Ortiz, R.; Cuesta, A.; Marquez, O. P.; Marquez, J.; Mendez, J. A.; Gutierrez, C. *J. Electroanal. Chem.* **1999**, *465*, 234.
(29) Orozco, G.; Gutierrez, C. *J. Electroanal. Chem.* **2000**, *484*, 64.
(30) Bjerke, A. E.; Griffiths, P. R.; Theiss, W. *Anal. Chem.* **1999**, *71*, 1967.
(31) Pirrung, M. C. *Chem. Rev.* **1997**, *97*, 473.
(32) Lam, K. S.; Salmon, S. E.; Hersh, E. M.; Hruby, V. J.; Kazmierski, W. M.; Knapp, R. J. *Nature* **1991**, *354*, 82.
(33) Xiang, X.-D.; Sun, X.; Briceno, G.; Lou, Y.; Wang, K.-A.; Chang, H.; Freedman, W. G.; Chen, S.-W.; Schultz, P. G. *Science* **1995**, *268*, 1738.
(34) Briceno, G.; Chang, H.; Sun, X.; Schultz, P. G.; Xiang, X.-D. *Science* **1995**, *270*, 273.
(35) Danielson, E.; Devenney, M.; Giaquinta, D. M.; Golden, J. H.; Haushalter, R. C.; McFarland, E. W.; Poojary, D. M.; Reaves, C. M.; Weinberg, W. H.; Wu, X.-D. *Science* **1998**, *279*, 837.
(36) Senkan, S.; Ozturk, S. *Angew. Chem.* **1999**, *111*, 867.
(37) Sun, S.-G.; Hong, S.-J.; Chen, S.-P.; Lu, G.-Q.; Dai, H.-P.; Xiao, X.-Y. *Sci. China, Ser. B* **1999**, *42*, 261.
(38) Gong, H.; Chen, S.-P.; Zhou, Z.-Y.; Sun, S.-G. *Chin. Sci. Bull.* **2001**, *46*, 1662.
(39) Budevska, B. O.; Griffiths, P. R. *Anal. Chem.* **1993**, *65*, 2983.
(40) Sun, S.-G. In *Electrocatalysis*; Lipkowski, J., Ross, P. N., Eds.; Wiley-VCH: New York, 1998; Chapter 6, p 243.
(41) Clavilier, J.; Faure, R.; Guinet, G.; Durand, R. *J. Electroanal. Chem.* **1980**, *107*, 205.
(42) Clavilier, J.; Durand, R.; Guinet, G.; Faure, R. *J. Electroanal. Chem.* **1981**, *127*, 281.
(43) Canullo, J. C.; Triaca, W. E.; Arvia, A. J. *J. Electroanal. Chem.* **1984**, *175*, 337.
(44) Canullo, J. C.; Triaca, W. E.; Arvia, A. J. *J. Electroanal. Chem.* **1986**, *200*, 397.
(45) Gomez, J.; Vazquez, L.; Baro, A. M.; Garcia, N.; Perdriel, C. L.; Triaca, W. E.; Arvia, A. J. *Nature* **1986**, *323*, 612.
(46) Arvia, A. J.; Canullo, J. C.; Custidiano, E.; Perdriel, C. L.; Triaca, W. E. *Electrochim. Acta* **1986**, *31*, 1359.
(47) Visintin, A.; Triaca, W. E.; Arvia, A. J. *J. Electroanal. Chem.* **1987**, *221*, 239.
(48) Kunimatsu, K.; Seki, H.; Golden, W. G.; Gorden, J. G., II; Philpott, M. R. *Surf. Sci.* **1985**, *158*, 596.
(49) Krauth, O.; Fahsold, G.; Magg, N.; Pucci, A. *J. Chem. Phys.* **2000**, *113*, 6330.
(50) Zhu, Y.; Uchida, H.; Watanabe, M. *Langmuir* **1999**, *15*, 8757.
(51) Gong, H.; Sun, S.-G.; Li, J. T.; Chen, Y.-J.; Chen, S.-P. *Electrochim. Acta* **2003**, *48*, 2933.
(52) Hoffmann, F. M. *Surf. Sci. Rep.* **1983**, *3*, 107.
(53) Bjerke, A. E.; Griffiths, P. R. *Appl. Spectrosc.* **2002**, *56*, 1275.